

# Patient-specific computational modelling, simulation and real-time processing for constrictive respiratory diseases.

Dr. Stavros Nousias

Version 1.00, July 2022

# About the author

**11.2022-Present**

**Post-Doctoral Research Associate**

Chair of Computational Modelling and Simulation  
Technical University of Munich  
Munich, Germany

**01.2020-10.2022**

**Research Associate**

Industrial Systems Institute  
Athena Research Center  
Marousi, Athens, Greece

**07.2016-12.2019**

**Research Assistant**

Visualization and Virtual Reality Lab  
Department of Electrical and Computer Engineering  
University of Patras, Greece  
Patras, Greece



# Overview

# Table of Contents

- 1 Overview
- 2 Introduction
- 3 Novelty and contribution
- 4 Novel patient-specific structural modelling
  - Computational modelling of the pulmonary system
  - Structural modelling
  - Bronchocontriction Simulation
  - Airflow flow in normal and constricted lungs
  - Human-machine interfaces for patient-specific pulmonary modelling
  - Applications
- 5 Monitoring medication adherence pulmonary diseases
  - Methodology
  - Data collection
  - Results
  - User interfaces for medication adherence monitoring and relevance feedback mechanism
- 6 Conclusion
- 7 Publications
- 8 References

# Introduction

# Introduction

## Asthma

- Asthma is a common chronic constrictive disease of the respiratory system
- Affects 500 million people worldwide <sup>1</sup>
- Societal cost
  - 56 billion dollars in 2011 in the USA
  - €19.3 billion in 2016 in the EU
- Inflammatory reaction leads to
  - airway remodelling
  - airflow limitation
  - diminished lung function

---

<sup>1</sup>Nunes, C., Pereira, A. M., Morais-Almeida, M. (2017). Asthma costs and social impact. *Asthma research and practice*, 3(1), 1-11.

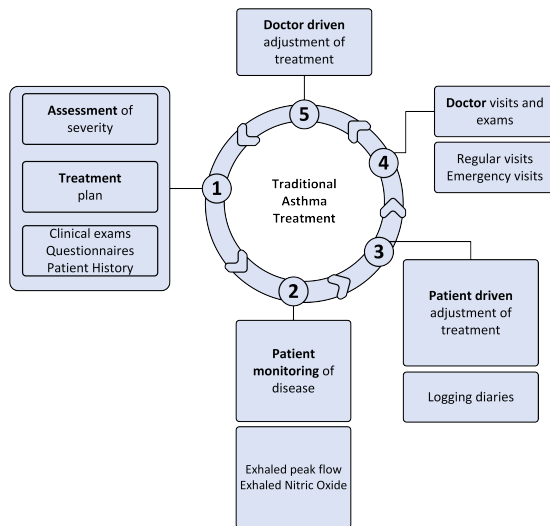
# Introduction

## Asthma

- Currently(Update 2022) there is no cure
- Treatment controls symptoms
- In general current therapies are still ineffective due to
  - insufficient understanding of pathophysiology
  - disease heterogeneity
- Recent studies indicate that a patient specific approach / patient-specific medicine is required

# Novelty and contribution

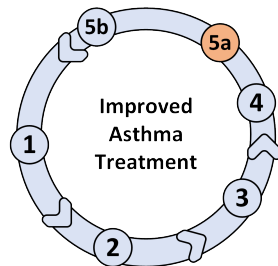
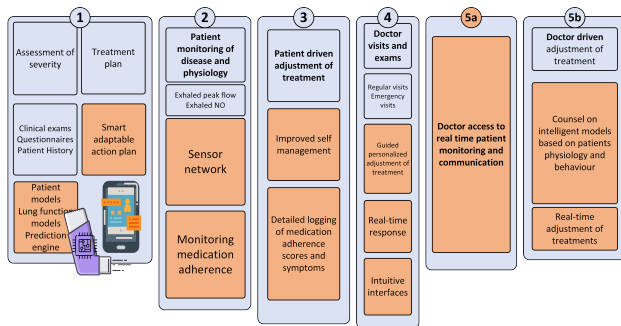
# Traditional asthma treatment



## Traditional approach

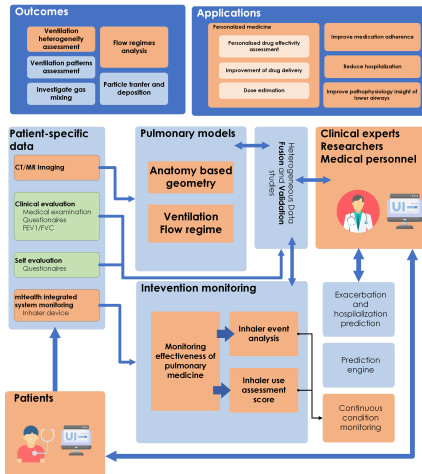
- initial diagnosis of the disease
- continuous cycle of readjustments
- clinical examination and questionnaires
- enrich patient's history

# Optimized asthma treatment





# Integrative models in clinical pulmonary research



The combination of pulmonary models and improved intervention monitoring guides medical personnel and the patient towards improved management of constrictive pulmonary conditions.

# Contribution I

- ① We generate validated 3D digital twins of pulmonary structures
- ② We introduce geometry processing methods that facilitate the simulation of bronchoconstriction.
- ③ Additionally, we perform CFD studies that quantify the airflow in normal and asthmatic patient-specific image-based 3-dimensional bronchial tree representations

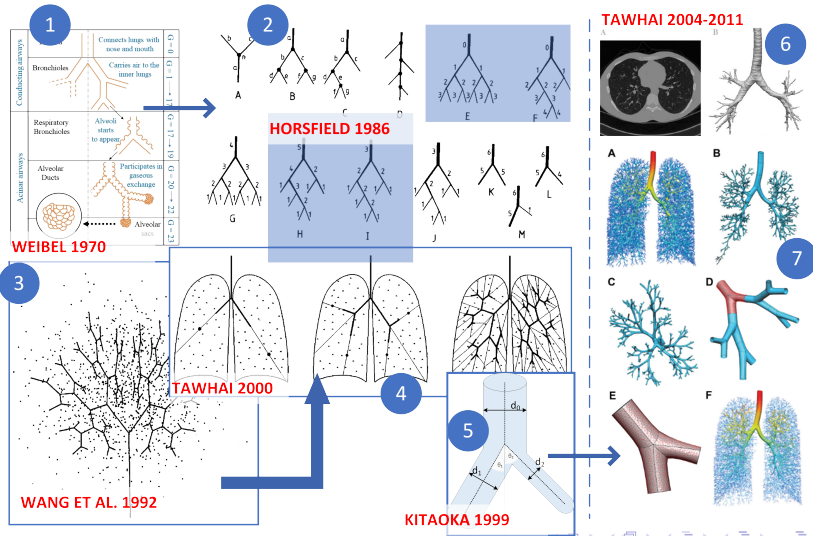
# Contribution II

- We investigate monitoring medication adherence through content based audio classification for pressurized metered dose inhalers.
- We compile two datasets containing inhaler use audio and present a comparative study investigating the classification accuracy of multiple machine and deep learning classifiers for a series of features.
- We propose a GMM based method that adequately differentiates inhaler events and in certain cases outperforms them.
- Furthermore, we present an approach driven by convolutional neural networks that adequately capture features and allow for computationally inexpensive real time embedded deployments

# Novel patient-specific structural modelling

# Related work, trends, challenges and applications

## Pulmonary structural modelling



## Related work, trends, challenges and applications

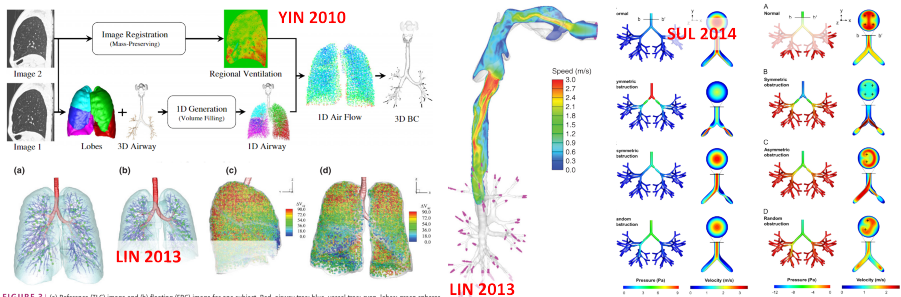
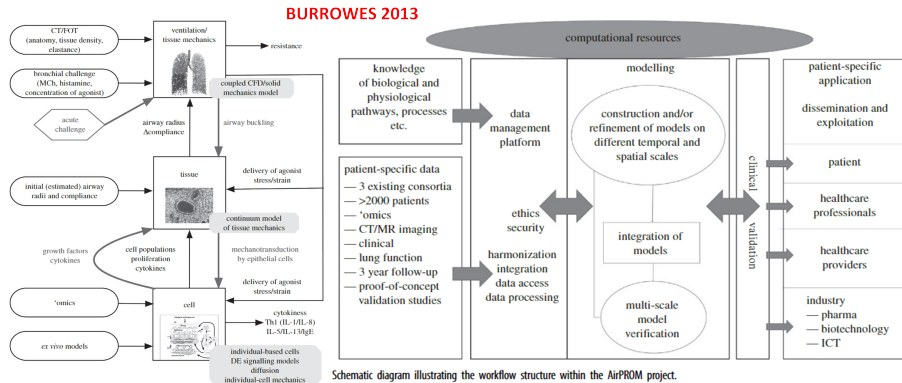


**FIGURE 3 |** (a) Reference (TLC) image and (b) floating (FRC) image for one subject. Red, airway tree; blue, vessel tree; cyan, lobes; green spheres, the landmarks at the bifurcations of the vessel tree. Registration-derived heterogeneous regional ventilation: (c) side view, (d) front view.

# Related work, trends, challenges and applications

## Multiscale models



# Related work, trends, challenges and applications

## Validation studies

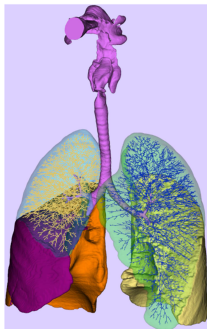


Table 2. Number of acini and generations between trachea and terminal bronchioles.

**MONTESANTOS 2016**

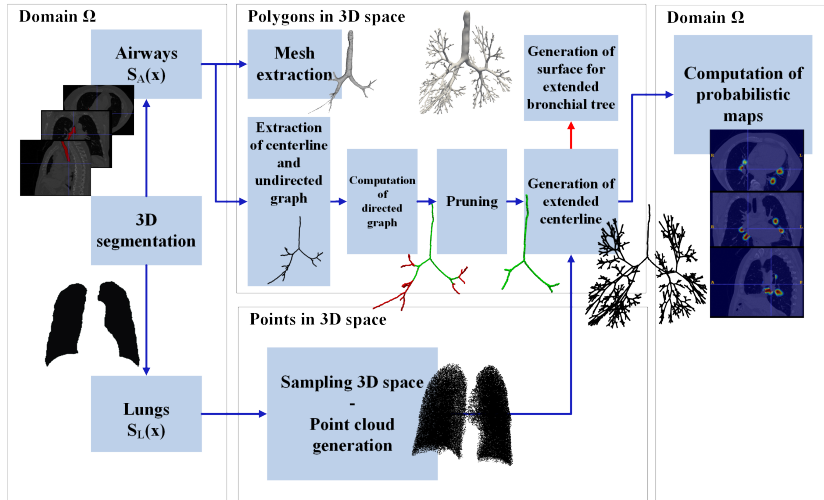
	No. of Acini	Generation distance of acini from trachea							
		RU	RM	RL	LU	LL	Lungs	min	max
Model	27763.6±7118.5	15.3±1.2	15.2±1.7	17.2±2.2	15.9±1.4	16.3±1.7	16.2±1.7	8	25
Weibel (1963)	66000						16	8	25
Horsfield (1968)	27992						14.6	8	25
Phalen (1978)		15	15	17	15	16	15.6		
Kitaoka (1999)	27706						17.6±3.4	8	23
Tawhai (2000)	29445	16.4	16	17.4	16.3	16.2	16	10	26
Florens (2011)	23000						15–16	9	23

Table 3. The branching, diameter and length ratios for Horsfield order ( $RB_H$ ,  $RD_H$ ,  $RL_H$ ) and Strahler order ( $RB_S$ ,  $RD_S$ ,  $RL_S$ ) respectively.

	$RB_H$	$RD_H$	$RL_H$	$RB_S$	$RD_S$	$RL_S$
Model	1.56 (0.98)	1.166 (0.99)	1.13 (0.77)	2.49 (0.99)	1.397 (0.99)	1.392 (0.99)
Phalen (1978)				2.508	1.351	1.333
Horsfield (1981)				2.51–2.81	1.35–1.45	1.33–1.46
Horsfield (1987)				2.54–2.81	1.5	1.55
Tawhai (2000)	1.39	1.109	1.14	2.358	1.323	1.344
Tawhai (2004)	1.47 (0.99)		1.13 (0.87)	2.8 (1.00)	1.41 (0.98)	1.39 (0.95)
Schmidt (2004)	1.48					

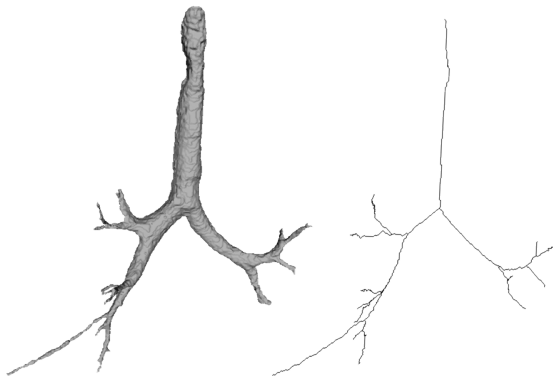
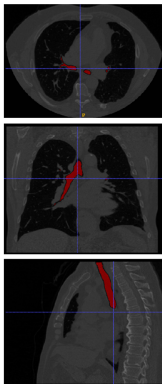


# Processing pipeline



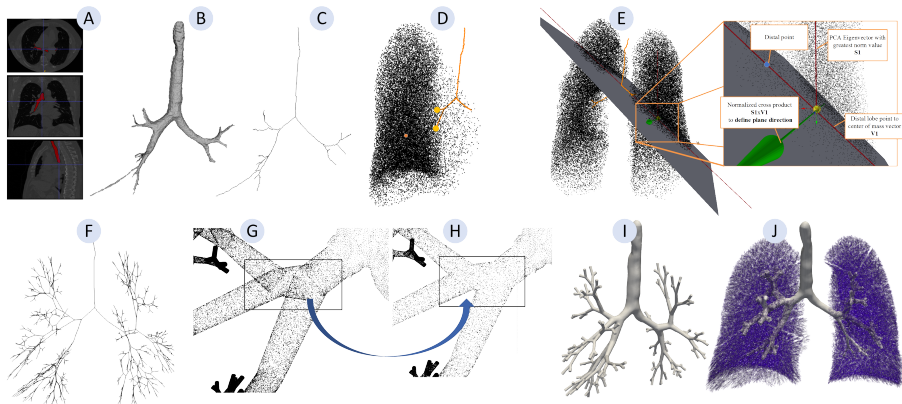
# Segmentation and one dimensional representation

- Extraction of airway surface and centerline from CT scans using the FAST framework.
- Airway segmentation (left) and airway surface generation(center) and generation of one-dimensional representation through skeletonization.



# Generation of extended bronchial tree

## • Bronchial tree extension process



# Generation of extended bronchial tree

I

The following steps can describe the bronchial tree extension algorithm.

For each lung subvolume  $S_{L_L}$  and  $S_{L_R}$ :

- ① Generate a point cloud sampling the subvolume with a uniform random process.
- ② Assign a seed point
- ③ Calculate the center of mass of the sampled points  $\mathbf{c} = \frac{\sum_{\mathbf{p}_i \in \mathcal{P}} \mathbf{p}_i}{|\mathcal{P}|}$
- ④ Employ principal component analysis (PCA) on the set of sampled points to define the splitting plane.  $\mathbf{D} = [\mathbf{p}_1 \ \mathbf{p}_1 \ \mathbf{p}_1 \ \cdots \ \mathbf{p}_n]$ ,  $\mathbf{A} = \mathbf{D}\mathbf{D}^T$  is the auto-correlation matrix.

Direct singular value decomposition yields  $\mathbf{A} = \mathbf{U}\mathbf{U}^T$  where  $\mathbf{U} = [\mathbf{u}_1 \ \mathbf{u}_2 \ \mathbf{u}_3]$  Then the largest eigenvector is defined as  $\mathbf{u}_m = \max_{1 \leq i \leq 3} \mathbf{u}_i$

- ⑤ Given the vector  $\mathbf{d}$  expressing the direction of the distal airway, the splitting plane is described by center of mass  $\mathbf{c}$  and vector  $\mathbf{d} \times [\mathbf{d} \times \mathbf{u}_m]$ . The selected plane maximizes the available space for each new subdivision.

# Generation of extended bronchial tree

II

- 1 Calculate the centroid of each new subdivision.
- 2 For each centroid, define a line segment starting from the seed point extending **40%** of the distance towards the centroid of the subdivision.
- 3 If a newly created branch is more minor than  $2mm$ , it is considered terminal.
- 4 The process is repeated until no seed points remain.
- 5 Any branch found outside the lung volume is removed along with children's branches.

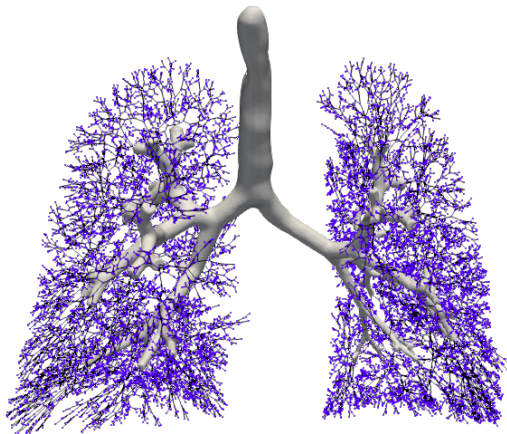
# Datasets

- VESSEL12 (VESsel SEgmentation in the Lung) challenge [Rudyanto et al., 2014] provides 20 anonymized scans in Meta (MHD/raw) format.

Scan	Image type	Pathology	Scanner and kernel	Spacing (mm)	Z-spacing (mm)	# Of slices	kV/mAs
01	Angio-CT	Alveolar inflammation	Siemens SOMATOM Sensation 64, B60f	0.76	1	355	120/40
02	Chest CT	Alveolar inflammation	Philips Mx8000 IDT 16, B Kernel	0.71	0.7	415	140/74
03	Chest CT	ILD	Philips Mx8000 IDT 16, B Kernel	0.62	0.7	534	120/77
04	LD Chest CT	ILD	Toshiba Aquilion ONE, FC55	0.86	1	426	100/44
05	Chest CT	ILD	Philips Mx8000 IDT 16, B Kernel	0.72	0.7	424	140/73
06	Angio-CT	ILD	Siemens SOMATOM Sensation 64, B30f	0.63	1	375	120/81
07	LD Chest CT	ILD	Toshiba Aquilion ONE, FC55	0.69	1	461	100/23

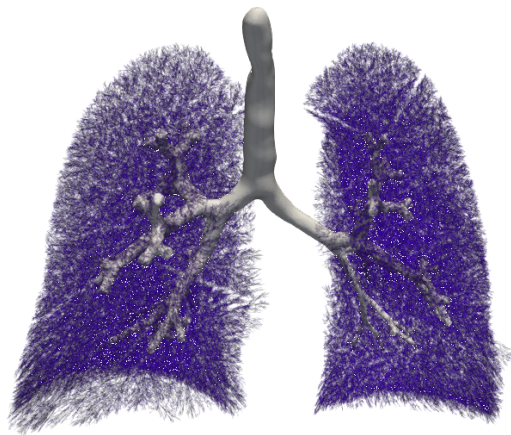
# Qualitative evaluation - 12 generations

Estimation of bronchial tree for 12 generations. Surface reconstruction was performed only for the first 7 generations



# Qualitative evaluation - 23 generations

Estimation of bronchial tree for 23 generations. Surface reconstruction was performed only for the first 7 generations





# Structural features comparison

	No of acini	Diameter Rate of Decline	$RB_H$	$RD_H$	$RL_H$	$RB_S$	$RD_S$	$RL_S$	Mean $\theta$
<b>AVATREE</b>	31204	$0.83 \pm 0.21$	1.74	1.259	$1.26 \pm 1.01$	2.35	1.25	$1.23 \pm 1.02$	$32.4488 \pm 28.95$
<b>Tawhai et al.2004</b>	29445		1.47		0.13	2.8	1.41	1.39	
<b>Horsfield et al.1986</b>	27992					2.54-2.81	1.5	1.55	37.28
<b>Bordas et al.2015</b>									$42.90 \pm 0.10$
<b>Montesantos et al. 2016</b>	$27763 \pm 7118.5$	$0.789 \pm 0.16$	1.56	1.116	1.13	2.49	1.397	1.392	$42.1 \pm 21.4$

# Strahler order comparison

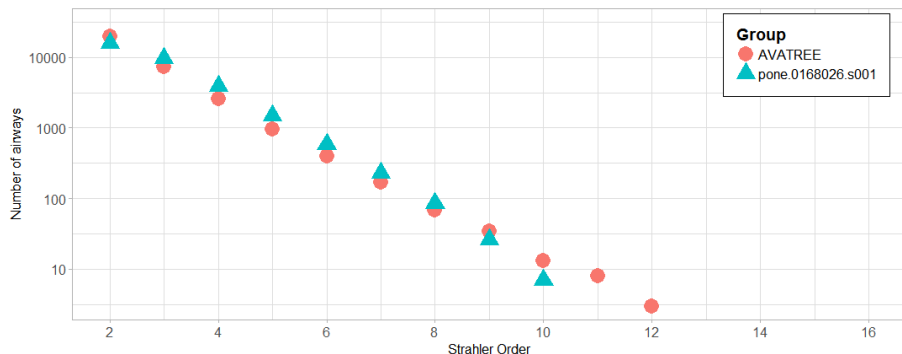


**Figure:** Comparison in terms of the number of airways for each level of Strahler orders. This comparison confirms that our model comes into agreement with *pone.0168026.s001*[Montesantos et al., 2016].

# Airway length distribution

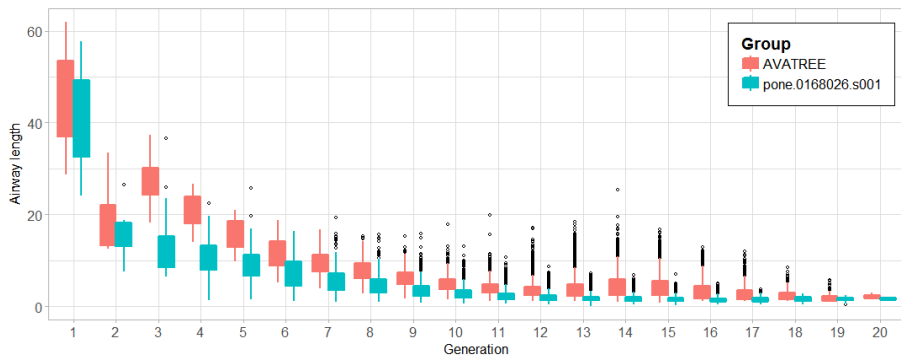


**Figure:** Distribution of airway lengths for each generation for AVATREE and *pone.0168026.s001* [Montesantos et al., 2016]

# Branching angle distribution

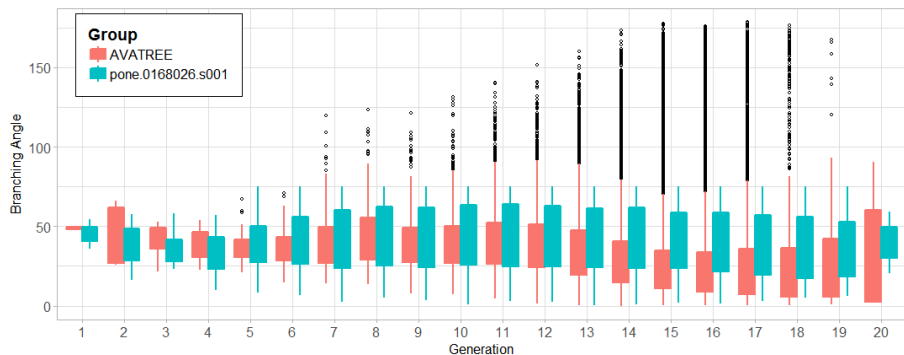


**Figure:** Distribution of branching angles for each generation as predicted by our model AVATREE [Nousias et al., 2020] and *pone.0168026.s001*

# Diameter distribution

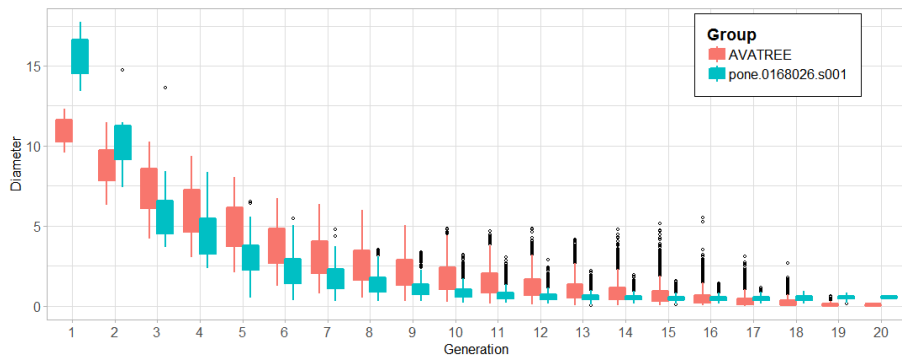


**Figure:** Distribution of diameters for each generation for AVATREE and *pone. 0168026.s001*

# Fundamentals on representation of 3D Geometry

## Preliminaries on 3D meshes

- Each triangular mesh  $\mathcal{M}$  can be described as  $\mathcal{M} = \{\mathcal{V}, \mathcal{E}, \mathcal{F}\}$   $\mathcal{V}$  is the set of vertices,  $\mathcal{E}$  is the set of edges, and  $\mathcal{F}$  is the set of faces
- Each vertex  $i$  can be represented as a point.

$$\mathbf{v}_i = (x_i, y_i, z_i), \forall i = 1, 2, \dots, N$$

- For each face  $\mathbf{f}_i$ ,  $\forall i = 1, 2, \dots, l$  we denote the centroid

$$\mathbf{m}_i = \frac{\mathbf{v}_{i_1} + \mathbf{v}_{i_2} + \mathbf{v}_{i_3}}{3}, \forall i = 1, 2, \dots, l$$

- The outward unit normal  $\mathbf{n}_{m_i}$  to the face  $\mathbf{f}_i$  (located at the centroid  $\mathbf{m}_i$ ) is calculated as  $\mathbf{n}_{m_i}$ :

$$\mathbf{n}_{m_i} = \frac{(\mathbf{v}_{i_2} - \mathbf{v}_{i_1}) \times (\mathbf{v}_{i_3} - \mathbf{v}_{i_1})}{\|(\mathbf{v}_{i_2} - \mathbf{v}_{i_1}) \times (\mathbf{v}_{i_3} - \mathbf{v}_{i_1})\|}, \forall i = 1, \dots, l$$

# Simulation of airway bronchoconstriction

- 1 Get vertex positions  $\mathbf{V}$
- 2 Initialize Laplacian matrix

$$\mathbf{L}_{i,j} = \begin{cases} \omega_{i,j} = \cot a_{ij} + \cot b_{ij}, & (i,j) \in E \\ \sum_{i,k \in E}^k -\omega_{ik}, & i = j \\ 0, & \text{otherwise} \end{cases} \quad (2)$$

- 3  $\delta = \mathbf{L}\mathbf{V} = [\delta_1^T, \delta_2^T, \dots, \delta_N^T]^T, \delta_i = -4A_i\kappa_i\mathbf{n}_i$
- 4 Initialize  $\mathbf{W}_L$  and  $\mathbf{W}_H$  in the following manner:

$$\mathbf{W}_L = k \cdot \mathbf{I} \cdot \sqrt{A} \mathbf{W}_H = \mathbf{I} \quad (3)$$

where  $\mathbf{I}$  is a unitary matrix,  $k$  a double constant set to  $10^{-3}$  and  $A$  the average face area of the model.

- 5 Solve for  $\mathbf{V}' \hat{\mathbf{V}} = \arg \min_{\mathbf{V}} \{ \|\mathbf{W}_L \mathbf{L} \mathbf{V}\|^2 + \mathbf{W}_H \|\mathbf{V} - \mathbf{V}_a\| \}$
- 6 Update  $\mathbf{W}_L$  and  $\mathbf{W}_H$  so that

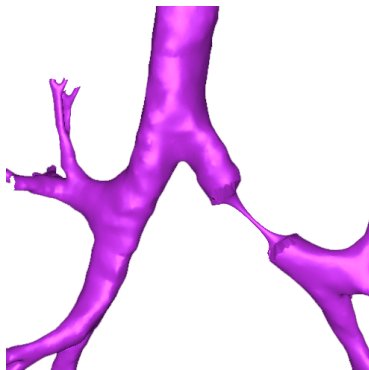
$$\mathbf{W}_L^{t+1} = s_L \cdot \mathbf{W}_L^t \mathbf{W}_H^{t+1} = \mathbf{W}_{H,i}^0 \cdot \sqrt{A_i^0/A_i^t} \quad (4)$$

where  $t$  denotes the iteration index.

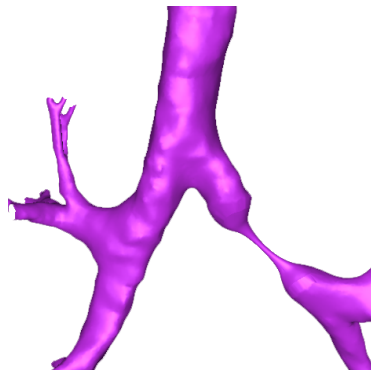
- 7 Recompute  $\mathbf{L}$ .
- 8 Compute narrowing ratio  $r^t$  through Shape Diameter Function[Shapira et al., 2008]
- 9 Repeat steps 4 to 7 for  $r^t > r + e$ , where  $r$  is the desired

# Addressing edge effects

- Addressing unwanted edge effects. The region between the narrowed and the unprocessed part is smoothed out using Taubin algorithm and Bilateral Normal filtering [Zheng et al., 2010]



(a)



(b)



# Simulation of airway constriction

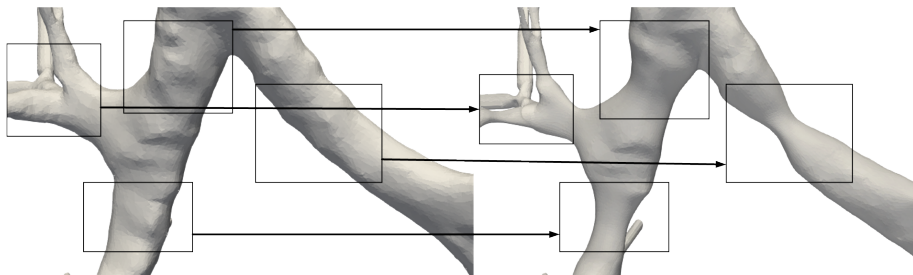
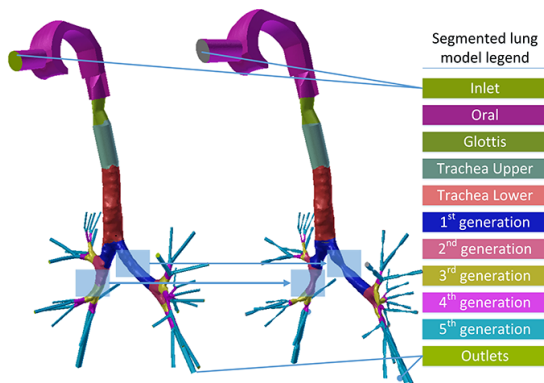


**Figure:** Simulation of constrictive pulmonary conditions. A selected region of the bronchial tree undergoes a controlled narrowing to the desired degree.

# Compute flow in normal and constricted lungs

## Geometry

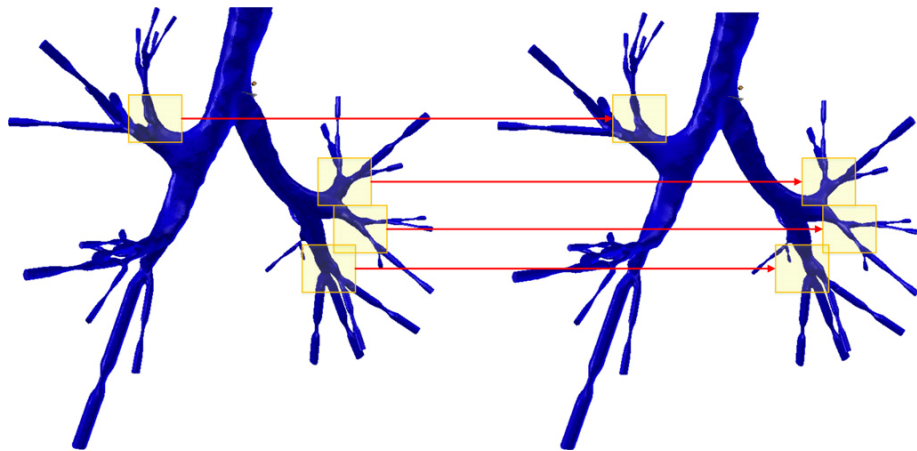
Visualization of bronchoconstriction simulation for the first five generations of a patient-specific reconstructed bronchial tree surface



# Compute flow in normal and constricted lungs

## Geometry

Visualization of bronchoconstriction simulation for the first 5 generations of a patient-specific reconstructed bronchial tree surface



# Compute flow in normal and constricted lungs

## Simulation setup

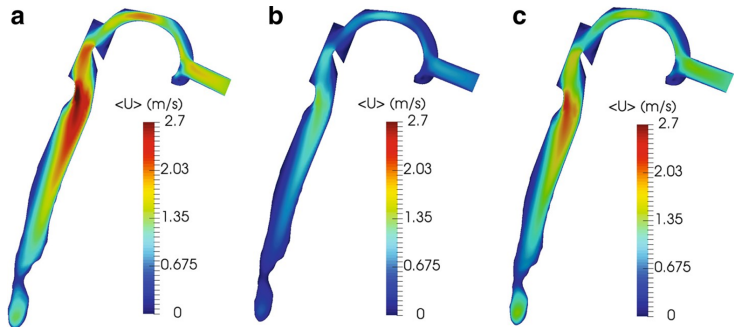
### OpenFOAM configuration

- Finite Volume Method
- SIMPLE scheme
- kOmegaSST turbulence model
- Pressure differential -15 Pa
- Time step  $5 \times 10^4$

# Compute flow in normal and constricted lungs

## Sagital cross-section

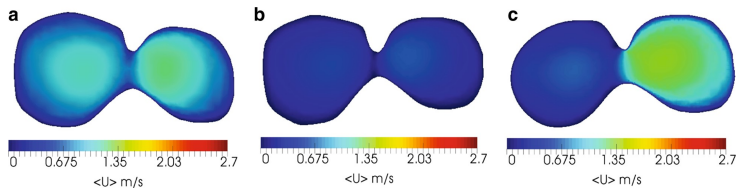
Sagital cross-section of oral cavity, glottis and trachea in three cases. Visualization of the airflow velocity profiles for a) Normal case b) Narrowing is introduced in both left and right lungs and c) narrowing is introduced only in the left lung.



# Compute flow in normal and constricted lungs

Cross-section, first bifurcation : Velocity profile

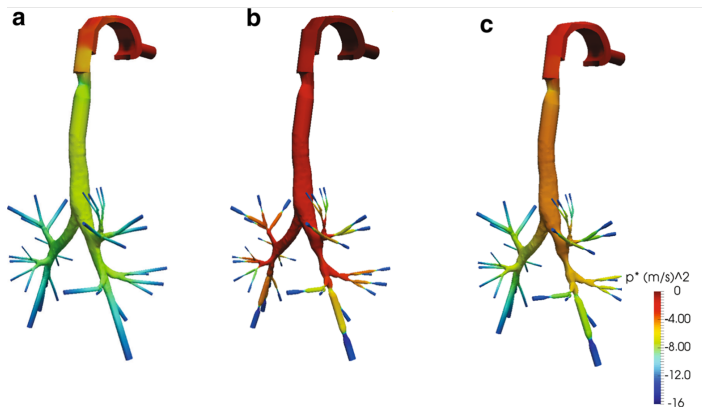
Velocity profile on the cross-section of the first bifurcation. a) Normal case  
b) Narrowing is introduced in both left and right lungs and c) narrowing is introduced only in the left lung.



# Compute flow in normal and constricted lungs

## Pressure distribution

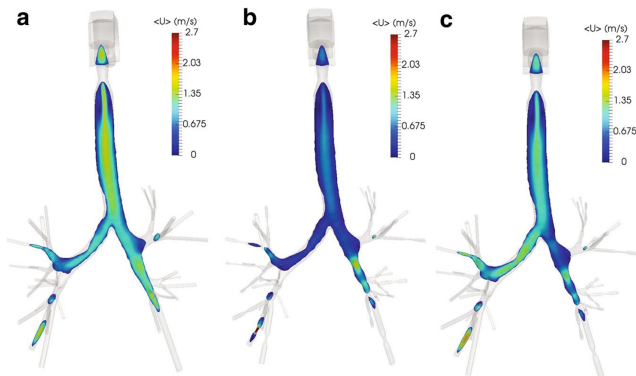
Pressure distribution for the surface of the oral cavity, glottis trachea and the first five generations. a. Normal case b. Narrowing introduced in both left and right lungs c. Narrowing is introduced only in the left lung.



# Compute flow in normal and constricted lungs

## Coronal cross section: Velocity profile

Visualization of velocity distribution for coronal cross-section normal and constricted lung geometry. a) Normal lung geometry b) Constrictions are introduced in both left and right lung airways c) Constrictions are introduced only on the left lung.





# Human-machine interfaces for patient-specific pulmonary modelling

User interface. The UI is comprised of four panels, namely the data input and output panel, area selection panel, segmentation panel and bronchoconstriction simulation panel

**Computational Modelling of the Lung and the Bronchial Tree**

**Load Model**

☒ Use brush | Brush Size: 200 | Brush distance: 1.00 | Nearest Neighbours

**Extend Selection**

**Segment by SDP**

Cone Angle: 0.00500 | Number of rays: 25

☒ Post processing | Per segment: | Number of clusters: 4 | Lambda: 0.00010

**Segment by generation**

**Narrow**

0%

Iterations: 8 | Contraction weight multiplier: 0.80

☐ Use custom function:  $\sin(x)$  | Frequency x PI: 0.20 | ☐ Use Interpolation | Factor: 0.50 | ☐ Extended smoothing

**Write**

**Reload**

**Export Selected Vertices To File**

**Export segmented model**

**Export model**

**Model import**

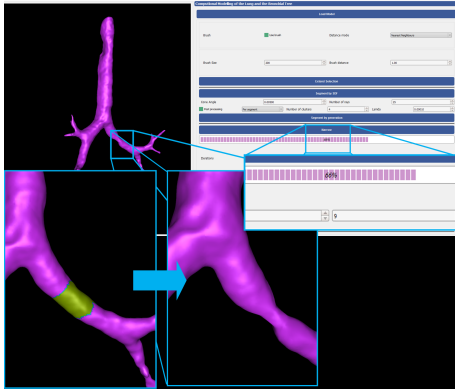
**Surface Segmentation Module**

**Bronchoconstriction Simulation Module**

**I/O Module**

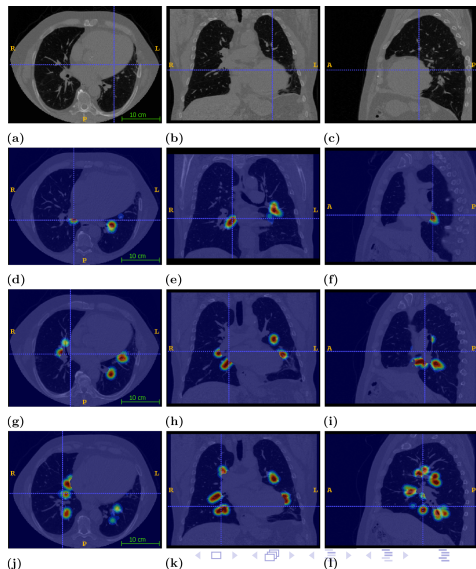
# Human-machine interfaces for patient-specific pulmonary modelling

Demonstration of broncho-constriction simulation. Airway of second generation narrowed at 34% of original diameter.



# Spatial probability pro generation

- Visualization of spatial likelihood for each branching generation
- Spatial maps are overlaid on the CT scans
- Probability to locate a branch of
  - 2nd generation
  - 3rd generation
  - 4th generation



# Monitoring medication adherence pulmonary diseases

# Prescribed inhaler use

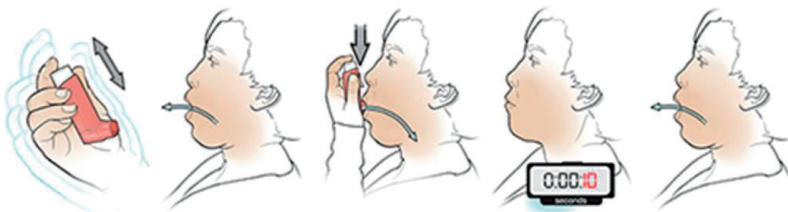


**Figure:** How to use a metered dose inhaler. A. The cap should be removed and the inhaler shaken B. The patient should breathe out, away from the inhaler C. The patient should bring the inhaler to the mouth, place it between the teeth and close the lips around it. Afterwards, the patient should start to breathe in slowly, press the top of the inhaler once, and keep breathing in slowly until a full breath is taken. D. The patient should remove the inhaler from the mouth, hold breath for about 10 seconds, and then breathe out. E. The patient should breathe out

# Related work, trends, challenges and applications

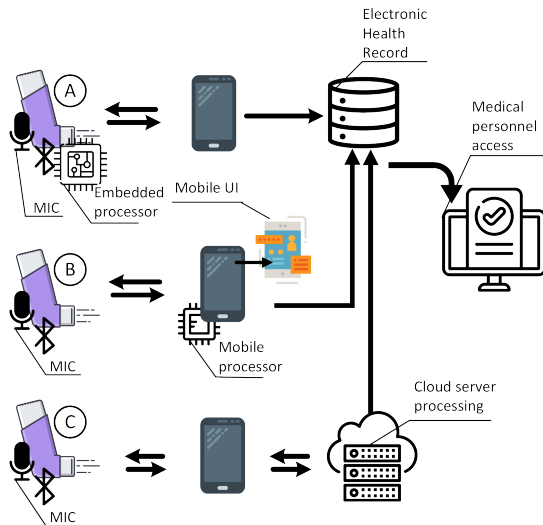
## Monitoring medication adherence

- **Howard et al.** [Howard et al., 2014] reported the existence of electronic or mechanical meters integrated into the device.
- **Holmes et al.**  
[Holmes et al., 2012, Holmes et al., 2013, Holmes et al., 2014] designed decision trees in the area of blister detection and respiratory sound classification.
- **Taylor et al.** [Taylor et al., 2014, Taylor et al., 2016] used the continuous wavelet transform to identify pMDI actuations in order to quantitatively assess the inhaler technique, focusing only on the detection of inhaler actuation sounds.
- **Taylor et al.** [Taylor et al., 2018] compared Quadratic Discriminant Analysis (QDA) and Artificial Neural Network (ANN) based classifiers using MFCC, Linear Predictive Coding, ZCR and CWT features.

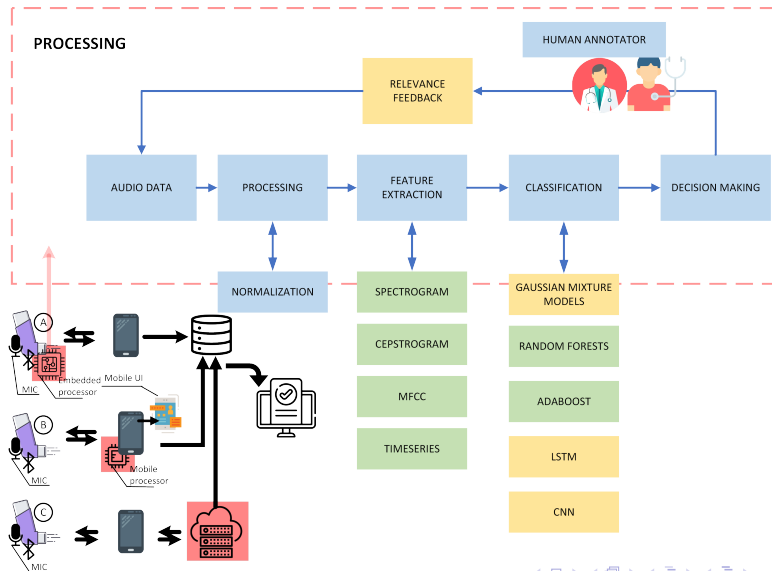
# System architecture

Monitoring system architecture.  
Three scenarios are taken into account.

- The inhaler device transmits the captured audio samples to the mobile device. The mobile device stores the audio files and sends them to a cloud processing server for differentiation.
- The audio device transmits the captured audio samples to the mobile device, and the differentiation occurs in the Mobile device processor.
- The captured audio is directly processed in the embedded processor.



# Audio processing pipeline





# Feature extraction

## Spectrogram

$$S = spectrogram\{x[n]\}(m, \omega) = |X(m, \omega)|^2 \quad (5)$$

where  $X(m, \omega)$  is the Fourier transform of  $x[n]$ ,

$$\omega \in (1, \dots, \frac{w}{2} + 1) \quad (6)$$

and

$$m \in (1, \dots, \left\lfloor \frac{N - (w - h)}{h} \right\rfloor) \quad (7)$$

$w$  is the window size and  $h$  is the frame increment. The latter is set to  $h = \frac{w}{4}$ .

Feature vector  $\mathbf{v}_s$

$$\mathbf{v}_s = \sum_{m=1}^M S(m, k) \quad (8)$$

$\mathbf{v}_s$  is subsequently downsampled to  $\mathbf{v}'_s$  so that

$$\mathbf{v}_s \in \mathcal{R}^{[\frac{w}{2}+1] \times [\frac{N-(w-h)}{h}]} \rightarrow \mathbf{v}'_s \in \mathcal{R}^{N_F \times [\frac{N-(w-h)}{h}]} \quad (9)$$

where  $N_F = 32$  is the number of frequencies after downsampling.

# Feature extraction

## Cepstrogram

Cepstrogram  $C(m, k)$  is formulated as

$$C(m, k) = \left| \sum_{n=0}^{N-1} \log |X(m, n)|^2 \cos\left(\frac{2\pi}{N} kn\right) \right|^2 \quad (10)$$

where  $X(m, n)$  is the short time Fourier transform,  $m$  denotes the  $m$ -th temporal component and  $k$  the  $k$ -th cepstral coefficient and  $n$  the  $n$ -th frequency component. The audio feature vector  $\mathbf{v} = [v_1 v_2 v_3 \dots v_k]$  is derived by summing up the quefrequency magnitude for every temporal window for each quefrequency component. Feature vector  $\mathbf{v}_c$

$$\mathbf{v}_c = \sum_{m=1}^M C(m, k) \quad (11)$$

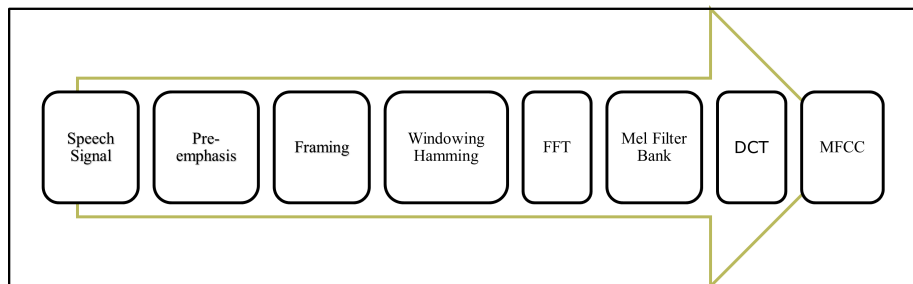
$\mathbf{v}_c$  is subsequently downsampled to  $\mathbf{v}'_c$  so that

$$\mathbf{v}_c \in \mathcal{R}^{[w/2+1] \times [N-(w-h)/h]} \rightarrow \mathbf{v}'_c \in \mathcal{R}^{N_F \times [N-(w-h)/h]} \quad (12)$$

# Feature extraction

## MFCC

MFCC is an efficient speech feature based on human hearing perceptions  
MFCC is based on known variation of the human ear's critical bandwidth with frequency.



# Feature extraction

Time

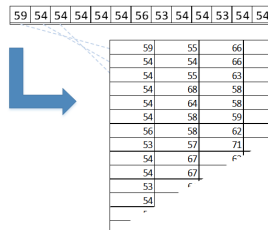
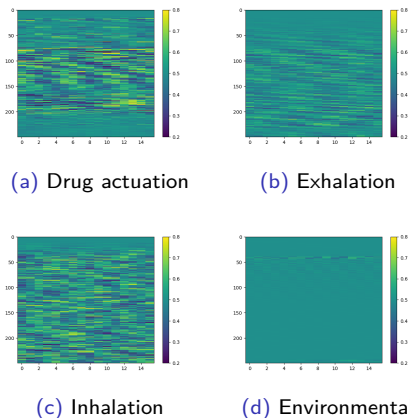


Figure: Illustration of reshaping of a vector into a two-dimensional matrix.

Figure: Visualization of the segmented

# Supervised feature classification with Gaussian Mixture Models

A Gaussian Mixture Model (GMM) :

$$\{a_i, \mu_i, \mathbf{C}_i\}, i \in K \quad (13)$$

The Gaussian mixture density:

$$p(\mathbf{v}|\theta_i) = \frac{1}{(2\pi)^{\frac{d}{2}} |\mathbf{C}_i|^2} e^{[-\frac{1}{2}(\mathbf{v}-\mu_i)^T \mathbf{C}_i^{-1}(\mathbf{v}-\mu_i)]} \quad (14)$$

The complete set of parameters for a mixture model with  $K$  components is

$$\Theta = \{a_1, \dots, a_K, \theta_1, \dots, \theta_K\} \quad (15)$$

Each GMM model  $\lambda_n$  for class  $n$  is parameterized as follows:

$$\lambda_n = \{a_k^n, \mu_k^n, \mathbf{C}_k^n\}, k = 1, \dots, K \quad (16)$$

An expectation maximization (EM) approach to derive the parameters  $K_n$  ,  $\{a_i, \mu_i, \mathbf{C}_i\}_n$  for the GMM  $\lambda_n$  corresponding to class  $n$  that best fit the input data

# Supervised feature classification with GMMs

## Expectation Maximization

E-step : We compute  $w_{ik}$  for all feature vectors  $\mathbf{v}_i$  and all mixture components  $k$ .

$$w_{ik} = \frac{p_k(\mathbf{v}_i, \theta_k) \cdot a_k}{\sum_{m=1}^K p_m(\mathbf{v}_i | \theta_m) \cdot a_m} \quad (17)$$

for all components  $k$ ,  $1 \leq k \leq K$  and all data samples  $i$ ,  $1 \leq i \leq N$ .

M-step: We calculate the new parameters. Given  $N_k = \sum_{i=1}^N w_{ik}$  the sum of membership weights for the  $k$  - *th* component we get the mixture weights:

$$a_k^{new} = \frac{N_k}{N}, 1 \leq k \leq K \quad (18)$$

The updated mean:  $\mu_k^{new} = \frac{1}{N_k} \sum_{i=1}^N w_{ik} \cdot \mathbf{v}_i, 1 \leq k \leq K$  and the updated

covariance:  $\mathbf{C}_k^{new} = \frac{1}{N_k} \sum_{i=1}^N w_{ik} (\mathbf{v} - \mu_i)^T (\mathbf{v} - \mu_i)$

Termination criteria:  $\log l(\Theta)_{t+1} - \log l(\Theta)_t \leq \epsilon$

where the log-likelihood, defined as  $\log l(\Theta) = \sum_{i=1}^N \log p(\mathbf{v}_i | \Theta)$  and  $\epsilon$  is a small user-defined scalar value.

# Supervised feature classification with GMMs

## Fitting

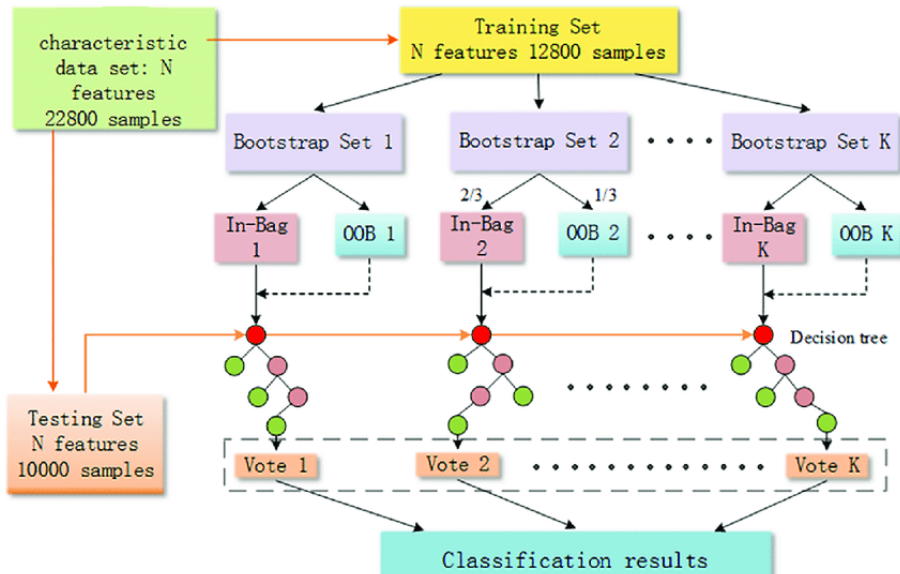
For each class of the data

- ① For  $K = 1 \cdots K_{max}$ 
  - ① For assumption that covariance matrix is either diagonal or full
    - ① Compute Gaussian Mixture
    - ② Compute Bayesian Information Criteria
  - ② GMM with lowest Bayesian Information Criteria is assumed to best fit the data

For test sample  $\mathbf{v}$  and for each GMM model compute likelihood.

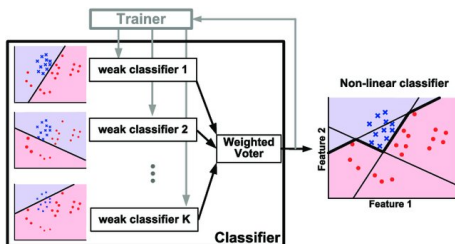
The test feature vector is assigned to the class with the greatest likelihood.

# Random Forest





# AdaBoost



Given:  $(x_1, y_1), \dots, (x_m, y_m)$  where  $x_i \in \mathcal{X}$ ,  $y_i \in \{-1, +1\}$ .

Initialize:  $D_1(i) = 1/m$  for  $i = 1, \dots, m$ .

For  $t = 1, \dots, T$ :

- Train weak learner using distribution  $D_t$ .
- Get weak hypothesis  $h_t : \mathcal{X} \rightarrow \{-1, +1\}$ .
- Aim: select  $h_t$  with low weighted error:

$$\varepsilon_t = \Pr_{i \sim D_t} [h_t(x_i) \neq y_i].$$

- Choose  $\alpha_t = \frac{1}{2} \ln \left( \frac{1 - \varepsilon_t}{\varepsilon_t} \right)$ .
- Update, for  $i = 1, \dots, m$ :

$$D_{t+1}(i) = \frac{D_t(i) \exp(-\alpha_t y_i h_t(x_i))}{Z_t}$$

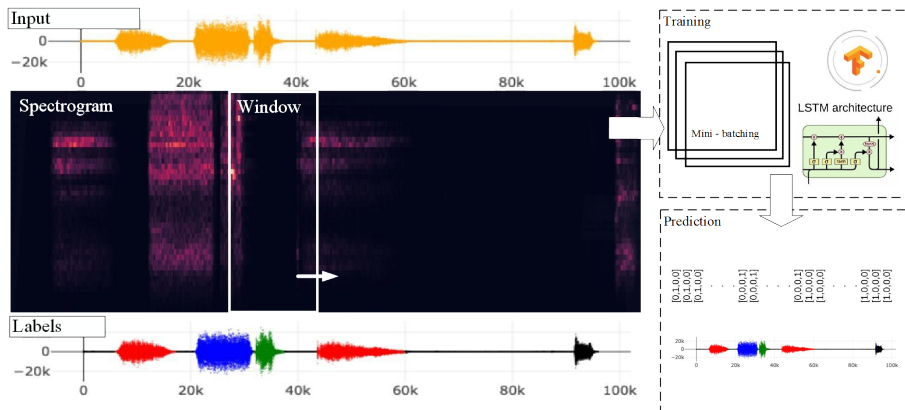
where  $Z_t$  is a normalization factor (chosen so that  $D_{t+1}$  will be a distribution).

Output the final hypothesis:

$$H(x) = \text{sign} \left( \sum_{t=1}^T \alpha_t h_t(x) \right).$$

Fig. 1 The boosting algorithm AdaBoost.

# Audio event classification and localization with long-short term memory recurrent neural networks



# Monitoring medication adherence through convolutional neural networks

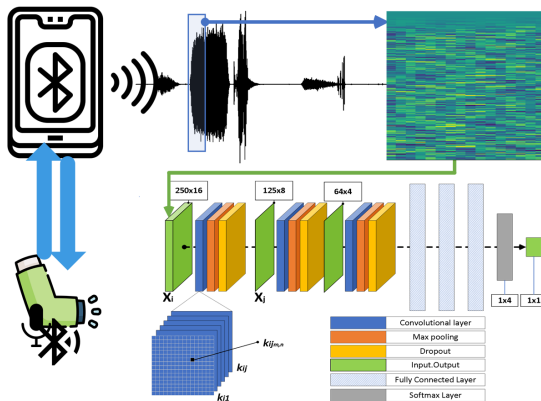


Figure: Overview of the processing pipeline

# Dataset A

- Inhaler sounds in indoor and outdoor environments
- 8 kHz sampling rate and 16-bit depth.
- Samsung HM1200 Bluetooth
- Placebo canisters.
- Mobile application connected to the Bluetooth microphone for data collection
- The sounds were categorized into inhaler actuations, exhalations, inhalations, and environmental or other sounds.
- Participation of 12 persons.
- In total, 1980 segments of 0.5 seconds each were compiled in a balanced collection,
- 495 per class.

# Dataset B

- Three subjects, between 28 and 34 years old,
- Placebo canisters.
- The first person (male) committed 240 audio files, the second subject (male), 70 audio files and the third subject (female) 50 audio files.
- 360 audio files
- **12 seconds each, containing a full inhaler usage case.**
- Acoustically controlled indoor environment
- protocol that defined all the essential steps of the pMDI inhalation technique.
- Monophonic audio at 8KHz , 16 bit

# Capturing device



(a)



(b)



(c)

**Figure:** a) Experimental setup of the pMDI. The Bluetooth microphone is firmly locked on the device. b) Inhaler prototype without casing. The pMDI is placed within a cavity. c) Inhaler prototype with casing.

# Annotation

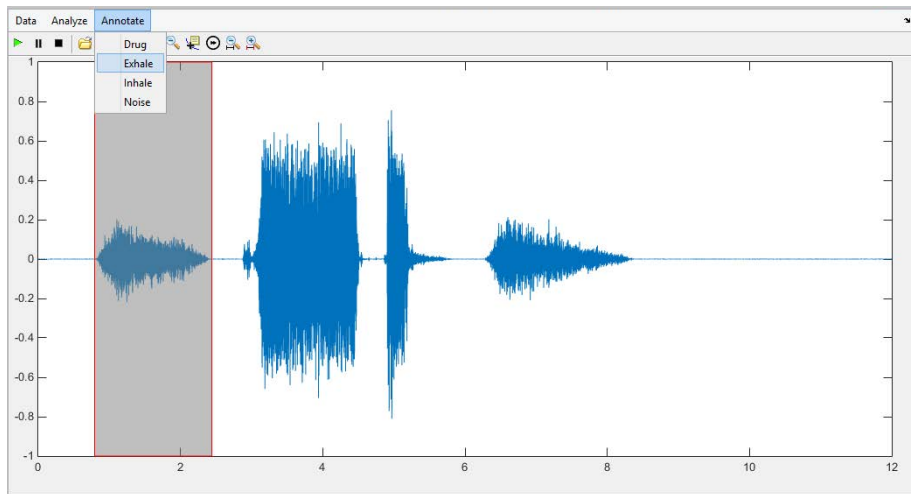
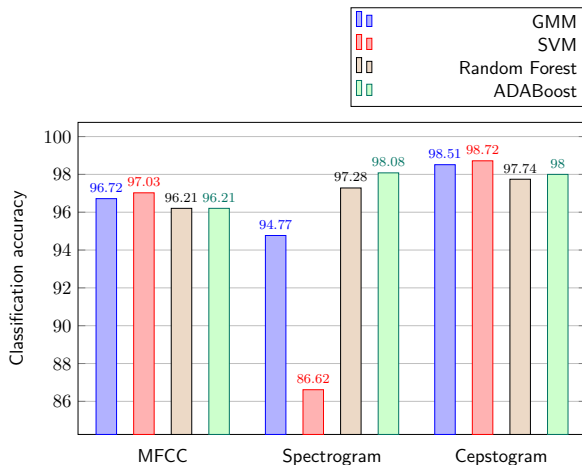


**Figure:** Annotation toolkit UI. The user inspects the audio graph, selects a segment corresponding to a certain class, and attaches the proper annotation.

# Classification accuracy for the 4-class problem. Dataset "A"





# Noise robustness assessment

**Table:** Classification accuracy (%) vs added noise factor

		Added noise and environmental sounds factor			
		0.00	0.10	0.20	0.50
MFCC	GMM	96.718	93.13	87.778	79.899
	SVM	97.026	93.59	87.0202	79.4444
	RF	96.205	93.23	86.2626	78.333
	ADA	96.205	92.93	85.9091	72
SPECT	GMM	94.768	92.83	88.384	78.485
	SVM	86.615	85.35	83.2323	78.68687
	RF	97.282	95.66	91.8182	83.28283
	ADA	98	95.15	92.0202	81.71717
CEPST	GMM	98.513	<b>96.47</b>	<b>96.414</b>	82.879
	SVM	<b>98.718</b>	95.81	91.9192	<b>83.93939</b>
	RF	97.744	95.91	92.7778	83.8889
	ADA	98	96.11	91.6667	81.9697
MFCC GMM FKL	ADA	96.718	91.364	87.172	78.131
SPECT GMM FKL	ADA	94.821	93.384	87.727	77.121
CEPST GMM FKL	ADA	98.513	94.242	94.444	81.162

# Confusion matrices

**Table:** Normalized % confusion matrix for MFCC, spectrogram and cepstrogram feature extraction approaches

			Reference											
			MFCC				SPECT				CEPST			
			Drug	Exhale	Inhale	Noise	Drug	Exhale	Inhale	Noise	Drug	Exhale	Inhale	Noise
Prediction	SVM	Drug	97.54	0.00	0.21	0.21	97.54	0.00	0.00	0.00	99.38	0.41	0.00	0.41
		Exhale	0.41	96.14	1.23	2.89	2.46	58.94	1.43	3.73	0.41	98.16	1.43	0.41
		Inhale	0.00	0.00	97.74	0.20	0.00	0.41	94.88	0.83	0.00	0.20	98.57	0.41
		Other	2.05	3.86	0.82	96.70	0.00	40.65	3.69	95.44	0.21	1.23	0.00	98.77
	RF	Drug	97.13	0.20	0.21	0.00	97.74	0.20	0.00	0.00	98.97	0.41	0.00	0.62
		Exhale	1.44	95.93	2.26	4.33	0.00	96.95	2.05	2.69	0.82	97.35	1.64	1.65
		Inhale	0.41	0.00	96.71	0.62	0.62	0.61	97.95	0.83	0.00	0.61	98.16	1.24
		Other	1.02	3.87	0.82	95.05	1.64	2.24	0.00	96.48	0.21	1.63	0.20	96.49
	ADA	Drug	97.54	0.00	0.00	0.41	98.77	0.41	0.00	0.00	99.18	0.20	0.20	0.21
		Exhale	1.03	96.75	1.65	4.95	0.41	96.95	1.43	1.45	0.62	97.35	1.84	1.03
		Inhale	0.00	0.20	96.91	1.03	0.00	0.20	98.36	0.62	0.00	0.61	97.54	0.82
		Other	1.43	3.05	1.44	93.61	0.82	2.44	0.21	97.93	0.20	1.84	0.42	97.94
	GMM	Drug	96.71	0.00	0.00	0.00	99.18	0.41	0.00	2.69	99.38	0.00	0.00	0.62
		Exhale	0.82	96.14	1.23	2.68	0.62	93.29	1.64	6.00	0.41	99.18	1.43	2.27
		Inhale	0.21	0.00	97.74	1.03	0.20	3.46	98.16	2.90	0.00	0.41	98.57	0.21
		Other	2.26	3.86	1.03	96.29	0.00	2.84	0.20	88.41	0.21	0.41	0.00	96.90

# Comparison to CWT

**Table:** Normalized % confusion matrix for continuous wavelet transform.

			Reference			
			CWT			
			Drug	Exhale	Inhale	Noise
Prediction	SVM	Drug	<b>97.11</b>	0.20	0.20	0.00
		Exhale	1.44	<b>98.16</b>	27.72	85.66
		Inhale	1.03	0.82	<b>71.66</b>	6.56
		Other	0.42	0.82	0.42	<b>7.78</b>
	RF	Drug	<b>98.97</b>	0.40	0.20	0.20
		Exhale	0.00	<b>94.10</b>	1.64	8.60
		Inhale	1.03	0.81	<b>95.70</b>	2.67
		Other	0.00	4.69	2.46	<b>88.53</b>
	ADA	Drug	<b>99.18</b>	0.00	0.41	0.41
		Exhale	0.00	<b>95.91</b>	1.64	6.56
		Inhale	0.20	0.61	<b>96.31</b>	1.64
		Other	0.62	3.48	1.64	<b>91.39</b>
ADA 2-Class			Drug		Other	
		Drug	<b>99.18</b>		0.27	
		Other	0.82		<b>99.73</b>	

# Relevance feedback

- 1 Require user defined entries

$$\mathcal{F} = \{\mathbf{v}_{F1}, \dots, \mathbf{v}_{Fn}, \dots, \mathbf{v}_{FN}\}$$

$$\text{Dataset } \mathcal{D} = \{\mathbf{v}_{D1}, \dots, \mathbf{v}_{Dm}, \dots, \mathbf{v}_{DM}\}$$

- 2 Initialize personalized dataset  $\mathcal{D}_F = \{\}$  as an empty set

- 3 For each  $\mathbf{v}_{Fn} \in \mathcal{F}$

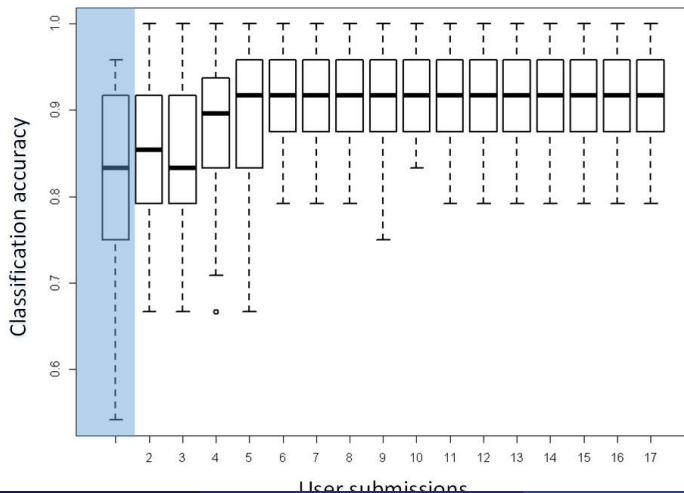
- $\mathcal{D}_{Fn} \leftarrow k$  nearest neighbors of  $\mathbf{v}_{Fn}$  using  $\mathcal{D}$   
 $\mathcal{D}_F = \mathcal{D}_F \cup \mathcal{D}_{Fn}$

- 4  $\mathcal{D}_F = \mathcal{D}_F \cup \mathcal{F}$

- 5 Ensure each element of  $\mathcal{D}_F$  is unique

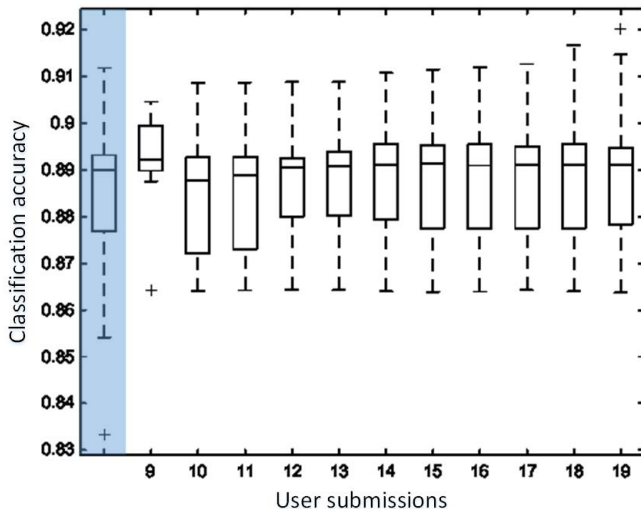
# Relevance feedback evaluation

## SVM CEPST



# Relevance feedback evaluation

## GMM CEPST



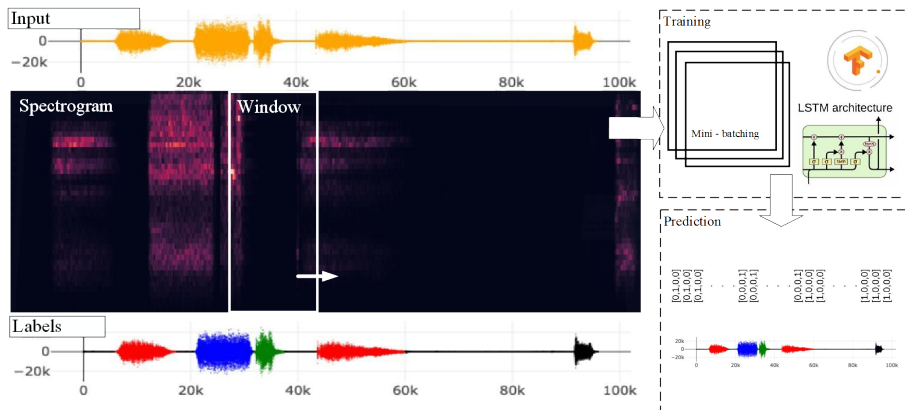
# Dataset B

- New features
  - Full recordings
  - Entail transition events
  - Per subject data organization
- Evaluation settings - per subject
  - Multi-subject
  - Single-subject
  - Leave One Subject Out
- Evaluation settings - per data input
  - Mixed
  - Non mixed

## Purpose

- Investigate model behaviour when training data are not enough
- Investigate transition between events
- Investigate intrasubject prediction accuracy

# Audio event classification and localization with long-short term memory recurrent neural networks





# Metrics

		Real	
		Positive	Negative
Predicted	Positive	True Positive (tp)	False Positive (fp)
	Negative	False Negative (fn)	True Negative (tn)

$$\text{accuracy} = \frac{(TP + TN)}{(TP + FP + TN + FN)} \quad (19)$$

$$\text{precision} = \frac{(TP)}{(TP + FP)} \quad (20)$$

$$\text{recall} = \frac{TN}{(TN + FP)} \quad (21)$$

# Results

## Accuracy

			Multi	LOSO	Single
Mixed	ada	cepst	92.11	90.35	90.67
	ada	mfcc	91.76	88.31	89.43
	ada	spect	89.8	84.55	88.79
	cnn	time	91.71	92.94	90.61
	gmm	cepst	89.81	80.54	89.33
	gmm	mfcc	82.83	82.12	78.49
	gmm	spect	86.45	83.58	86.88
	lstm	spect	92.16	87.73	91.1
	rf	cepst	91.69	90.28	91.05
	rf	mfcc	91.61	89.36	90.86
	rf	spect	89.47	85.7	89.85
	svm	cepst	91.67	82.34	90.89
	svm	mfcc	92.49	87.29	92.14
	svm	spect	34.03	34	33.53

			Multi	LOSO	Single
Non-mixed	ada	cepst	95.02	93.32	92.57
	ada	mfcc	95.91	87.02	93.8
	ada	spect	94.01	84.92	92.99
	cnn	time	95.29	94.12	92.69
	gmm	cepst	94.1	80.92	94.02
	gmm	mfcc	76.48	79.39	68.82
	gmm	spect	86.81	81.49	86.52
	lstm	spect	92.93	88.89	92.54
	rf	cepst	93.92	91.98	93.3
	rf	mfcc	94.87	90.08	93.26
	rf	spect	92.79	85.5	93.26
	svm	cepst	95.15	77.67	94.57
	svm	mfcc	96.21	83.97	96.23
	svm	spect	75.32	69.85	77.09

# Results

## F1 Score

			Drug			Exhale			Inhale		
			LOSO	Multi	Single	LOSO	Multi	Single	LOSO	Multi	Single
Non-mixed	ada	cepst	63.64	93.02	92.93	94.25	95.98	93.18	96.17	96.41	93.77
	ada	mfcc	40	96.43	94.77	91.4	96.15	94.09	84.76	96.72	94.03
	ada	spect	56	95.38	94.91	85.98	93.89	92.7	90.75	95.79	93.43
	cnn	time	70	82.8	85.84	95.23	96.3	93.58	98.24	96.77	96.2
	gmm	cepst	62.5	93.16	94.85	88.37	94.92	94.26	74.23	96.38	96
	gmm	mfcc		10.78	18.43	81.72	83.02	76.11	48.1	66.32	75.89
	gmm	spect	47.06	94.36	95.14	81.6	85.48	83.73	92.95	93.13	88.58
	lstm	spect	69.8	93.24	92.97	89.9	93.55	93.19	92.93	94.08	94.03
	rf	cepst	84.21	92.35	92.9	91.61	94.57	94.24	97.07	96.1	94.47
	rf	mfcc	74.07	93.61	93.8	89.95	95.68	93.58	95.24	95.48	95.26
	rf	spect	66.67	94.9	95.72	86.03	92.57	92.73	93.51	95.15	94.47
	svm	cepst	43.9	93.81	94.59	78.28	96.05	95.3	83.25	95.79	96.04
	svm	mfcc	47.62	96.18	96.76	86.85	96.54	96.62	85.31	96.24	95.76
	svm	spect	81.82	95.96	96.81	75.37	76.28	75.89	95.36	94.98	94.24

# Results

## F1 Score

			Drug			Exhale			Inhale		
			LOSO	Multi	Single	LOSO	Multi	Single	LOSO	Multi	Single
Mixed	ada	cepst	17.58	64.84	63.28	83.57	87.27	84.45	86.6	89.24	86.79
	ada	mfcc	11.87	64.1	65.51	82.46	86.67	81.03	80.55	89.46	85.42
	ada	spect	25.89	74.85	74.5	72.77	81.48	78.43	84.73	91.19	88.94
	cnn	time	21.85	58.1	63.41	89.08	86.81	83.06	94.94	89.95	89.05
	gmm	cepst	25.81	63.96	67.46	72.42	83.73	81.02	48.3	84.74	85.21
	gmm	mfcc		17.13	0.47	72.12	73.85	65.76	41.62	53.86	53.32
	gmm	spect	32.78	73.59	74.27	67.42	72.78	74.44	89.34	89.13	85.89
	lstm	spect	23.1	66.61	70.67	75.5	86.4	83.21	86.04	90	88.87
	rf	cepst	25.41	63.22	64.73	83.01	86.55	84.77	86.6	89.19	89.38
	rf	mfcc	15.87	59.78	63.84	82.57	86.97	84.88	84.69	87.57	87.01
	rf	spect	30.98	73.69	75.91	74.26	80.86	80.83	88.41	90.65	90.27
	svm	cepst	11.42	62.82	65.09	68.1	86.9	84.8	68.26	88.92	88.77
	svm	mfcc	12.83	59.93	66.03	79.33	88.91	87.66	80.38	88.93	88.66
	svm	spect	25.59	71.28	73.71	40.93	37.5	35.19	89.51	90.98	89.73

# Results

Performance evaluation : Comparison of the computational cost

Method	Classification execution time	Feature extraction Time	Sum
cnn-time	0.000460227	0.000968868	0.0014
lstm-spect	0.000700771	0.001955032	0.0027
gmm-spect	1.82257E-05	0.018367229	0.0184
ada-spect	0.000773556	0.018398599	0.0192
rf-spect	0.000278274	0.019732354	0.02
svm-spect	4.70897E-05	0.02074642	0.0208
svm-mfcc	2.1926E-05	0.021171822	0.0212
rf-mfcc	0.000275223	0.021114178	0.0214
gmm-mfcc	2.35955E-05	0.023210378	0.0232
ada-mfcc	0.000852494	0.022573248	0.0234
rf-cepst	0.000272068	0.051282082	0.0516
gmm-cepst	1.19811E-05	0.054902331	0.0549
ada-cepst	0.0008844	0.055359981	0.0562
svm-cepst	3.10628E-05	0.057136457	0.0572

# Results

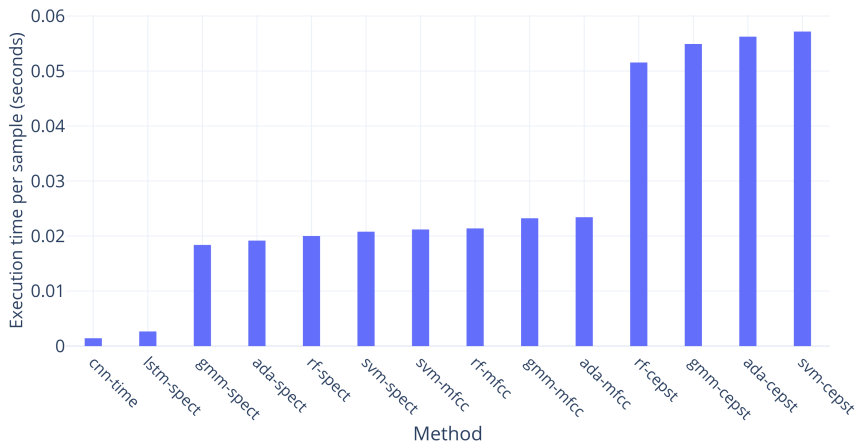
## Others

**Table:** Classification accuracy in relevant state of the art

Method	Drug	Inhale	Exhale
Holmes et al. (2012) [Holmes et al., 2012]	89	-	-
Holmes et al. (2013-14) [Holmes et al., 2013, Holmes et al., 2014]	92.1	91.7	93.7
Taylor et al. (2017) / QDA [Taylor et al., 2018]	88.2	-	-
Taylor et al. (2017) / ANN [Taylor et al., 2018]	65.6	-	-

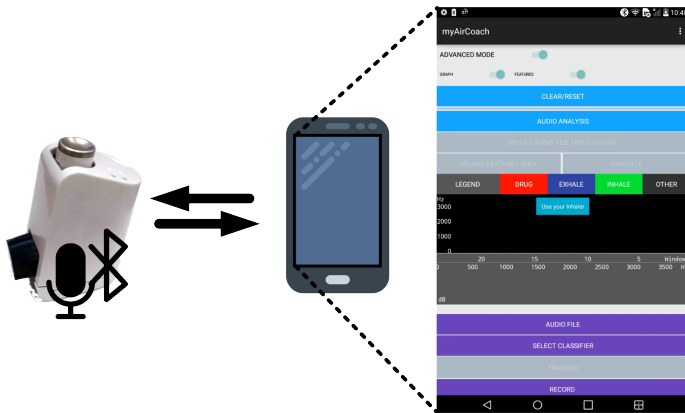
# Results

Performance evaluation : Comparison of the computational cost



# User interfaces for medication adherence monitoring and relevance feedback mechanism

Visualization of the relation between the inhaler device, the mobile device and the application.

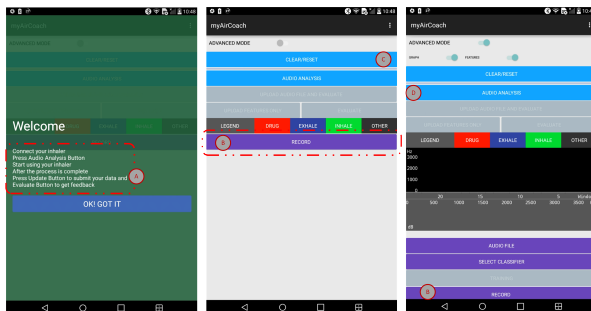




# User interfaces for medication adherence monitoring and relevance feedback mechanism

## Basic features and views

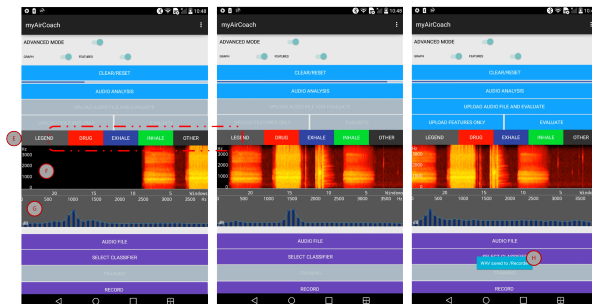
A) Welcoming screen and guidelines B) Record button to start audio capturing from the inhaler device. C) Clear/Reset functionality to restart the application. D) Audio analysis to classify the audio data.



# User interfaces for medication adherence monitoring and relevance feedback mechanism

## Basic features and views

E) Color legend. F) Spectrogram visualization. G) Spectrogram audio features for the given window under processing. H) "WAV saved" signal to notify the user that the audio file has been captured.



# Conclusion

# Conclusion

- This dissertation lies in the family of approaches that constitute the virtual physiological human
- Aims to provide novel methods that facilitate patient-specific computational modelling of the pulmonary system within the scope of Asthma.
- Additional data-driven machine and deep learning methodologies are discussed that contribute to the improvement of self-management of Asthma.
- Computational models contribute to personalized medicine
- Smart devices provide further evidence to improve self management

# Publications

# Publications in Journals

- ❶ **Nousias S**, Zacharaki EI, Moustakas K. AVATREE: An open-source computational modelling framework modelling Anatomically Valid Airway TREE conformations. PloS one. 2020 Apr 3;15(4):e0230259.
- ❷ **Nousias S**, Lalos AS, Arvanitis G, Moustakas K, Tsirelis T, Kikidis D, Votis K, Tzovaras D. An mHealth system for monitoring medication adherence in obstructive respiratory diseases using content based audio classification. IEEE Access. 2018 Feb 26;6:11871-82.
- ❸ Ntalianis V, Fakotakis ND, **Nousias S**, Lalos AS, Birbas M, Zacharaki EI, Moustakas K. Deep CNN Sparse Coding for Real Time Inhaler Sounds Classification. Sensors. 2020 Jan;20(8):2363.
- ❹ Lalas A, **Nousias S**, Kikidis D, Lalos A, Arvanitis G, Sougles C, Moustakas K, Votis K, Verbanck S, Usmani O, Tzovaras D. Substance deposition assessment in obstructed pulmonary system through numerical characterization of airflow and inhaled particles attributes. BMC medical informatics and decision making. 2017 Dec;17(3):25-44.
- ❺ Fakotakis ND, **Nousias S**, Arvanitis G, Zacharaki EI, Moustakas K. Revisiting Audio Pattern Recognition for Asthma Medication Adherence: Evaluation with the RDA Benchmark Suite. IEEE Access, under review.

# Conferences

- 1 Ntalianis V, **Nousias S**, Lalos AS, Birbas M, Tsafas N, Moustakas K. Assessment of medication adherence in respiratory diseases through deep sparse convolutional coding. In: IEEE Conference on Emerging Technologies and Factory Automation. Vol 2019-Sept. Zaragoza, Spain: IEEE; 2019: 1657-1660. doi:10.1109/ ETFA.2019.8869054
- 2 Pettas D, **Nousias S**, Zacharaki EI, Moustakas K. Recognition of breathing activity and medication adherence using lstm neural networks. In 2019 IEEE 19th International Conference on Bioinformatics and Bioengineering (BIBE) 2019 Oct 28 (pp. 941-946). IEEE.
- 3 Arvanitis G, Kocsis O, Lalos AS, **Nousias S**, Moustakas K, Fakotakis N. 3-Class Prediction of Asthma Control Status Using a Gaussian Mixture Model Approach. In Proceedings of the 10th Hellenic Conference on Artificial Intelligence 2018 Jul 9 (pp. 1-2).
- 4 Lalas A, Kikidis D, Votis K, Tzovaras D, Verbanck S, **Nousias S**, Lalos A, Moustakas K, Usmani O. Numerical assessment of airflow and inhaled particles attributes in obstructed pulmonary system. In 2016 IEEE International Conference on Bioinformatics and Biomedicine (BIBM) 2016 Dec 15 (pp. 606-612). IEEE. BibTeX
- 5 **Nousias S**, Lakoumentas J, Lalos A, Kikidis D, Moustakas K, Votis K, Tzovaras D. Monitoring asthma medication adherence through content based audio classification. In 2016 IEEE symposium series on computational intelligence (SSCI) 2016 Dec 6 (pp. 1-5). IEEE.
- 6 **Nousias S**, Lalos AS, Moustakas K. Computational modeling for simulating obstructive lung diseases based on geometry processing methods. In International Conference on Digital Human Modeling and Applications in Health, Safety, Ergonomics and Risk Management 2016 Jul 17 (pp. 100-109). Springer, Cham.
- 7 **Nousias S**, Lalos A, Moustakas K, et al. Computational modeling methods for simulating obstructive human lung diseases. In: 9.1 Respiratory Function Technologists/Scientists. Vol 48. London: European Respiratory Society; 2016:PA4401. doi:10.1183/13993003.congress-2016.PA4401

# Other Publications

## • Autonomous driving

- Nousias S, Pikoulis E, Mavrokefalidis C, Lalos AS, Moustakas K. Accelerating 3D scene analysis for autonomous driving systems. In: IEEE International Conference on Very Large Scale Integration. ; 2021.
- Nousias S, Pikoulis EV, Mavrokefalidis C, Lalos AS. Accelerating deep neural networks for efficient scene understanding in automotive cyber-physical systems. IEEE Int Conf Ind Cyber-Physical Syst. 2021.

## • 3D processing

- Nousias S, Arvanitis G, Lalos AS, Moustakas K. Fast mesh denoising with data driven normal filtering using deep variational autoencoders. IEEE Transactions on Industrial Informatics. 2020 Jun 8;17(2):980-90.
- Nousias S, Arvanitis G, Lalos AS, Moustakas K. Mesh Saliency Detection Using Convolutional Neural Networks. In: 2020 IEEE International Conference on Multimedia and Expo (ICME). IEEE; 2020:1-6.  
doi:10.1109/ICME46284.2020.9102796



# Other Publications

## • Heritage science

- Nousias S, Arvanitis G, Lalos AS, et al. A Saliency Aware CNN-Based 3D Model Simplification and Compression Framework for Remote Inspection of Heritage Sites. IEEE Access. 2020;8(1):169982-170001. doi:10.1109/access.2020.3023167

## • Gamification

- Tselios C, Nousias S, Bitzas D, Amaxilatis D, Akrivopoulos O, Lalos AS, Moustakas K, Chatzigiannakis I. Enhancing an eco-driving gamification platform through wearable and vehicle sensor data integration. In European Conference on Ambient Intelligence 2019 Nov 13 (pp. 344-349). Springer, Cham.
- Nousias S, Tselios C, Bitzas D, Amaxilatis D, Montesa J, Lalos AS, Moustakas K, Chatzigiannakis I. Exploiting gamification to improve eco-driving behaviour: The GameCAR approach. Electronic Notes in Theoretical Computer Science. 2019 May 4;343:103-16.
- Lalos AS, Nousias S, Moustakas K. GameCAR: Gamifying Self Management of Eco-driving. ERCIM News Spec Theme Digit Twins. 2018.
- Nousias, S. Lalos, A., Tselios, C., Bitzas, D., Amaxilatis, D., Chatzigiannakis, I., Gerasimos, A. and Moustakas, K. Gamification of EcoDriving Behaviours through Intelligent Management of Dynamic Car and Driver Information. DOI: 10.5220/0008862301000123 In OPPORTUNITIES AND CHALLENGES for European Projects (EPS Portugal 2017/2018 2017), pages 100-123 ISBN: 978-989-758-361-2

# Other Publications

- Virtual Physiological human

- Papoulias G, Nousias S, Moustakas K. Simulation framework for fluid-solid interaction of cerebral aneurysm wall deformation. In: International Conference on Information, Intelligence, Systems and Applications. Vol 0. ; 2019:0-0.

- Missing data handling

- Nousias S, Tselios C, Bitzas D, et al. Managing nonuniformities and uncertainties in vehicle-oriented sensor data over next-generation networks. In: 2018 IEEE International Conference on Pervasive Computing and Communications Workshops (PerCom Workshops). IEEE; 2018:272-277. doi:10.1109/PERCOMW.2018.8480342
- Nousias S, Lalos AS, Kalogeras A, Alexakos C, Koulamas C, Moustakas K. Sparse modelling and optimization tools for energy-efficient and reliable IoT. In: 2019 1st International Conference on Societal Automation, SA 2019. Krakow, Poland; 2019. doi:10.1109/SA47457.2019.8938029
- Nousias S, Tselios C, Bitzas D, Lalos AS, Moustakas K, Chatzigiannakis I. Uncertainty Management for Wearable IoT Wristband Sensors Using Laplacian-Based Matrix Completion. In: 2018 IEEE 23rd International Workshop on Computer-Aided Modeling and Design of Communication Links and Networks (CAMAD). Vol 2018-Sept. IEEE; 2018:1-6. doi:10.1109/CAMAD.2018.8515001

## References

# References I



Holmes, M. S., D'Arcy, S., Costello, R. W., and Reilly, R. B. (2013). An acoustic method of automatically evaluating patient inhaler technique.

*In 2013 35th Annual International Conference of the IEEE Engineering in Medicine and Biology Society (EMBC)*, pages 1322–1325. IEEE.



Holmes, M. S., D'arcy, S., Costello, R. W., and Reilly, R. B. (2014). Acoustic analysis of inhaler sounds from community-dwelling asthmatic patients for automatic assessment of adherence.

*IEEE journal of translational engineering in health and medicine*, 2:1–10.

# References II



Holmes, M. S., Le Menn, M., D'Arcy, S., Rapcan, V., MacHale, E., Costello, R. W., and Reilly, R. B. (2012).

Automatic identification and accurate temporal detection of inhalations in asthma inhaler recordings.

*Proceedings of the Annual International Conference of the IEEE Engineering in Medicine and Biology Society, EMBS*, pages 2595–2598.



Howard, S., Lang, A., Patel, M., Sharples, S., and Shaw, D. (2014).  
Electronic monitoring of adherence to inhaled medication in asthma.  
*Current Respiratory Medicine Reviews*, 10(1):50–63.



Montesantos, S., Katz, I., Pichelin, M., and Caillibotte, G. (2016).  
The creation and statistical evaluation of a deterministic model of the human bronchial tree from hrct images.  
*PLOS one*, 11(12):e0168026.

# References III



Nousias, S., Zacharaki, E. I., and Moustakas, K. (2020).  
Avatree: An open-source computational modelling framework  
modelling anatomically valid airway tree conformations.  
*PloS one*, 15(4):e0230259.



Rudyanto, R. D., Kerkstra, S., Van Rikxoort, E. M., Fetita, C., Brillet, P.-Y., Lefevre, C., Xue, W., Zhu, X., Liang, J., Öksüz, İ., et al.  
(2014).  
Comparing algorithms for automated vessel segmentation in computed  
tomography scans of the lung: the vessel12 study.  
*Medical image analysis*, 18(7):1217–1232.



Shapira, L., Shamir, A., and Cohen-Or, D. (2008).  
Consistent mesh partitioning and skeletonisation using the shape  
diameter function.  
*The Visual Computer*, 24(4):249.

# References IV



Taylor, T. E., Holmes, M. S., Sulaiman, I., Costello, R. W., and Reilly, R. B. (2016).

Monitoring inhaler inhalations using an acoustic sensor proximal to inhaler devices.

*Journal of aerosol medicine and pulmonary drug delivery*, 29(5):439–446.



Taylor, T. E., Holmes, M. S., Sulaiman, I., D'Arcy, S., Costello, R. W., and Reilly, R. B. (2014).

An acoustic method to automatically detect pressurized metered dose inhaler actuations.

*Conference proceedings : ... Annual International Conference of the IEEE Engineering in Medicine and Biology Society. IEEE Engineering in Medicine and Biology Society. Annual Conference*, 2014:4611–4614.

# References V



Taylor, T. E., Zigel, Y., De Looze, C., Sulaiman, I., Costello, R. W., and Reilly, R. B. (2018).

Advances in audio-based systems to monitor patient adherence and inhaler drug delivery.

*Chest*, 153(3):710–722.



Zheng, Y., Fu, H., Au, O. K.-C., and Tai, C.-L. (2010).

Bilateral normal filtering for mesh denoising.

*IEEE Transactions on Visualization and Computer Graphics*, 17(10):1521–1530.